

Spin-Rotated states as a basis for Non-Orthogonal Configuration Interaction: A Size-Consistent Variational Approach

Nicholas Lee¹ and Alex J. W. Thom¹

¹Yusuf Hamied Department of Chemistry, Lensfield Road, Cambridge, CB2 1EW, U.K.

April 20, 2022

Abstract

Spin contamination is a problem that plagues the Unrestricted Hartree–Fock (UHF) method. This paper proposes a method to obtain the spin-pure components from a symmetry broken UHF (sb-UHF) solution using Non-Orthogonal Configuration Interaction (NOCI). Current NOCI methods often use a set of states selected based on chemical intuition. We define a Spin-Rotated-NOCI (SR-NOCI) in which Spin-Rotated states generated from a single sb-UHF state are used as a basis for NOCI. This approach is demonstrated to be size-consistent and to produce spin pure states. We demonstrate the method using molecular hydrogen and ethene as model systems. We also study the dissociation of ethene into carbenes employing Absolutely Localised Molecular Orbitals (ALMOs) and find that we are able to obtain spin pure states at all geometries.

1 Introduction

Hartree–Fock theory is a mean-field approach where each electron interacts with the averaged field generated by all other electrons[1]. However, the mean-field approach is an approximation and need not, in general, respect the symmetries of the electronic Hamiltonian[2]. As such, the self-consistent solutions found using the Hartree–Fock equations may not respect these same symmetries, leading to symmetry breaking[3–5]. A classic example comes from Unrestricted Hartree–Fock (UHF) where the α and β spin orbitals are allowed to be described with different spatial functions. This typically leads to a symmetry broken UHF (sb-UHF) solution[6] at a lower energy level than the Restricted Hartree–Fock (RHF) solution.

When modelling not just a simple molecule, but a dissociating one, it is well-known[7] that the Restricted Hartree–Fock (RHF) description of a molecular system often breaks down as bonds dissociate. The Unrestricted Hartree–Fock (UHF) description gives a more accurate representation of the dissociation, but the UHF solutions are not in general eigenfunctions of \hat{S}^2 . While the UHF solution gives a lower energy and is thus a closer approximation to the true ground state wave function by the variational principle, it comes at the cost of spin contamination[8, 9]. Both the examples of a simple molecular system and a dis-

sociating one are a manifestations of what Löwdin referred to as the *Symmetry Dilemma*[10].

Spin contamination is also a serious concern when attempting to assign spin states in a molecular system. For example, in singlet fission research[11–15], the singlet-triplet gap is of paramount importance as it determines the thermodynamics, and hence feasibility of the fission. An accurate prediction of the singlet-triplet gap is current being sought after in the field, and so there is a great desire to obtain states with a well-defined total spin.

Ideally, we seek a method that gives spin states with good quantum numbers, is size-consistent and scales well with system size. To that end, there have been quite a number of approaches developed. Projected Hartree–Fock[16, 17] and Half-Projection methods[18–22] were developed to restore various symmetries such as spin and particle numbers. These are known as Variation after Projection (VAP) approaches. Another promising method for producing spin eigenstates is Neuscamman’s Jastrow-modified Antisymmetric Geminal Power (JAGP)[23], and brings on other desirable properties such as size-extensivity and polynomial scaling. However, the implementation of this procedure is challenging.

In contrast we propose a method where the symmetry is restored after a variational approach, so share the philosophy of Projection after Variation (PAV). However, using NOCI, the symmetry restoration pro-

jection is performed variationally using a Configuration Interaction, so we denote our methods Variational Projection after Variation (VPAV).

Recently, our group has reported the use of Hartree-Fock (HF) solutions found by SCF metadynamics[24, 25] as a basis for Non-Orthogonal Configuration Interaction[26, 27]. We refer to such an approach to NOCI as multi-state NOCI (MS-NOCI) to reflect its use of multiple SCF states. HF solutions were used as they are more chemically relevant to the system in question. However, because it is based on the sb-UHF states, this approach may not produce spin states with correct spin symmetry even after a judicious selection of HF solutions. With an aim to generate spin symmetry-respecting states in a general fashion, we demonstrate that using multiple spin-rotations of a single HF state as a basis for NOCI, hereafter known as spin-rotated NOCI (SR-NOCI), is a general and size-consistent method for spin restoration of symmetry broken HF states.

It should be noted that the use of spin rotation for spin projection is not new[28–30]. Furthermore, the use of spin-rotated states as a basis for NOCI has previously been attempted by Sundstrom and Head-Gordon[31], and more recently by Nite and Jimenez-Hoyos[32]. This work aims to generalise the approach to dissociating systems and differs from the latter publication in that symmetry-projection is performed through NOCI, without the need for grid-integration. It also generalises the approximate spin projection methods currently in use[33–35]. To the best of our knowledge, a comprehensive study on the feasibility of spin-rotated states as a basis for NOCI has not previously been attempted.

The remainder of the paper is structured as follows: Section 2 introduces the theory behind the approach and shows that this approach is formally size-consistent. Section 3 considers the method applied to the hydrogen molecule and its dimer, while Section 4 studies the dissociation of ethene. Section 5 compares the results from MS-NOCI against SR-NOCI. We conclude with a summary of the applicability of this method.

Notation	Description
χ_μ	Atomic orbital μ , where $1 \leq \mu \leq M$ for molecule A and $M + 1 \leq \mu \leq M + N$ for molecule B.
U, V	Single determinant wave functions of complete system of two coupled molecules, A and B.
$U^A, U^B,$ V^A, V^B	Single determinant wave functions of the respective molecules A and B, in states U and V.
u_i, v_i	Spin orbitals belonging to the states U and V, respectively. $1 \leq i \leq P$ for molecule A and $P + 1 \leq i \leq P + Q$ for molecule B.
$c^k_{\cdot i}, d^l_{\cdot j}$	Expansion coefficients for spin orbitals u_i and v_j , respectively, in terms of basis orbitals χ_k and χ_l .
S_{UV}^A, S_{UV}^B	Overlap matrices between states U and V on molecule A and on molecule B, respectively.
$D(i j)$	Cofactor of determinant D with row i and column j removed.
\hat{F}	One-electron component of the Hamiltonian.
\hat{G}	Two-electron component of the Hamiltonian.
$\hat{R}(\theta, \hat{n})$	Spin rotation operator of angle θ about axis \hat{n} .
S_{AB}	Overlap matrix of the complete system of molecules A and B.
S_A, S_B	Overlap matrix of molecule A and B, respectively.
H_{AB}	Hamiltonian matrix of the complete system of molecules A and B.
H_A, H_B	Hamiltonian matrix of molecule A and B, respectively.

Table 1: Notation used. Most of the notation used follows I. Mayer³⁶

2 Theory

2.1 General approach

To restore the required spin-symmetry, we begin with a sb-UHF state, and perform multiple spin rotations on it to obtain a set of spin-rotated states. The spin-rotated states will thus serve as the basis for NOCI. In the case of a dimer, we first localise the spin orbitals onto each molecule (which doesn’t affect the overall wavefunction) and perform spin rotations on each of its constituent molecules independently of each other. If sufficient rotations are chosen, the

set of spin-rotated states is expected to span the spin space sufficiently such that a linear combination of these states will have good spin quantum numbers. The mathematical details of this approach are elaborated upon in this section. The notation used for the rest of the paper is summarised in Table 1. Where necessary, we employ Head-Gordon *et al.*'s tensor notation[37].

2.2 Generator Coordinate Method (GCM)

The GCM has been widely used in nuclear physics since the 1930s to restore symmetry to symmetry-broken wave functions[38–41]. Recently, work by Scuseria and co-workers used the method in Projected Hartree–Fock theory[17]. As such, a derivation of generalised eigenvalue equation from the ansatz of GCM shall not be included. We shall only point out the important aspects of the derivation.

For arbitrary spin state P , let state Q be a spin-rotation of it, $|Q\rangle = \hat{R}(\theta, \hat{n})|P\rangle$, such that state Q is related to state P by a spin rotation θ about axis \hat{n} . The matrix elements of the Hamiltonian and Overlap between P and Q can then be expressed as:

$$\begin{aligned} H_{pq} &= \langle P | \hat{H} | Q \rangle \\ &= \langle P | \hat{H} \hat{R}(\theta, \hat{n}) | P \rangle \end{aligned} \quad (1)$$

$$\begin{aligned} S_{pq} &= \langle P | Q \rangle \\ &= \langle P | \hat{R}(\theta, \hat{n}) | P \rangle \end{aligned} \quad (2)$$

and define square matrices \mathbf{H} and \mathbf{S} respectively. We may create a variationally optimized combination of these states by solving the resulting generalised eigenvalue equation:

$$\sum_q H_{pq} D_{qi} = \sum_q S_{pq} D_{qi} E_i \quad (3)$$

for each reference state P . This corresponds to the NOCI equation with spin rotated states of P as the non-orthogonal basis, giving us an early indication that NOCI serves as a discretised version of the GCM and hence a viable candidate for restoring spin symmetry.

2.3 Generating Spin-Rotated States

For a rotation about the axis $\hat{n} = (n_x, n_y, n_z)$ by an angle θ , we define the spin rotation matrix \mathbf{R} in the basis of (α, β) as:

$$\begin{aligned} \mathbf{R} &= \begin{pmatrix} \cos \frac{\theta}{2} - in_z \sin \frac{\theta}{2} & (-n_y - in_x) \sin \frac{\theta}{2} \\ (n_y - in_x) \sin \frac{\theta}{2} & \cos \frac{\theta}{2} + in_z \sin \frac{\theta}{2} \end{pmatrix} \\ &= \begin{pmatrix} R_{11} & R_{12} \\ R_{21} & R_{22} \end{pmatrix} \end{aligned} \quad (4)$$

This matrix performs spin rotation on each spin orbital of a state. For a multi-electron state P and its spin-rotated form $Q = \mathbf{R}P$, we can express them in spinor form (The basis is expressed as the direct product of the spatial basis and the two-component spin basis) as follows[42]:

$$\begin{aligned} \begin{pmatrix} Q_\alpha \\ Q_\beta \end{pmatrix} &= \mathbf{R} \begin{pmatrix} P_\alpha \\ P_\beta \end{pmatrix} \\ &= \begin{pmatrix} R_{11}P_\alpha + R_{12}P_\beta \\ R_{21}P_\alpha + R_{22}P_\beta \end{pmatrix} \end{aligned} \quad (5)$$

where we have partitioned the (Generalized Hartree–Fock (GHF)) orbitals of states P and Q into their spin components. P_α and P_β are both matrices of dimensions $n_{AO} \times n_e$ such that n_{AO} is the number of atomic orbitals in the given basis and n_e is the total number of electrons. For an initial UHF state, for example, P_α consists of a block corresponding to the α orbitals, and contains zeroes for the β orbitals. Q_α and Q_β are similarly matrices of dimensions $n_{AO} \times n_e$, corresponding to the alpha spin and beta spin components respectively. By stacking Q_α and Q_β together as a $2n_{AO} \times n_e$ matrix, each column corresponds to a GHF orbital.

To obtain a corresponding direct-product basis for a dimer, spin rotation would have to be performed on each of the component molecules independently. This would entail localising orbitals on each of the molecules and performing spin rotation on them separately. While this could be accomplished with localisation techniques such as Boys[43] or Pipek-Mezey[44], these approaches break down when the molecular separation in the dimer is small.

As such, we turn to using Absolutely Localised Molecular Orbitals (ALMOs)[45, 46]. Using the ALMO SCF method, the orbitals in a UHF state are always localised on one of the two molecules, even when they are very close. At larger separations between molecules, the ALMO solutions become equivalent to the conventional localized UHF solutions.

2.4 Proof of Size-Consistency

We consider the case where molecules A and B are far apart, such that $\langle \chi_\mu | \chi_\nu \rangle = 0$ if:

1. $1 \leq \mu \leq M$ and $M + 1 \leq \nu \leq M + N$, or
2. $1 \leq \nu \leq M$ and $M + 1 \leq \mu \leq M + N$

i.e. if the two basis orbitals are localized on different molecules.

2.4.1 Inner product of spin orbitals

We express the spin orbitals which make up states U and V as a linear combination of basis orbitals.

$$u_i = \sum_{\mu}^{M+N} \chi_{\mu} c_{i,\mu}^{\mu} \quad (6)$$

$$v_j = \sum_{\nu}^{M+N} \chi_{\nu} d_{j,\nu}^{\nu} \quad (7)$$

The spin orbitals are expressed in the combined basis of molecules A and B, but are localized so they describe either molecule A or B, and the properties of the terms in the equation are summarised in Table 2.

In this basis of orbitals describing **both** molecules A and B, the coefficients of the orbitals describing B will be zero on the spin orbitals centered on A and vice versa.

Taking the inner product of the two spin orbitals,

$$\begin{aligned} \langle u_i | v_j \rangle &= \sum_{\mu=1}^{M+N} \sum_{\nu=1}^{M+N} c_{i,\mu}^{*\mu} \langle \chi_{\mu} | \chi_{\nu} \rangle d_{j,\nu}^{\nu} \\ &= \sum_{\mu=1}^M \sum_{\nu=1}^M c_{i,\mu}^{*\mu} \langle \chi_{\mu} | \chi_{\nu} \rangle d_{j,\nu}^{\nu} \\ &\quad + \sum_{\mu=M+1}^{M+N} \sum_{\nu=1}^M c_{i,\mu}^{*\mu} \langle \chi_{\mu} | \chi_{\nu} \rangle d_{j,\nu}^{\nu} \\ &\quad + \sum_{\mu=1}^M \sum_{\nu=M+1}^{M+N} c_{i,\mu}^{*\mu} \langle \chi_{\mu} | \chi_{\nu} \rangle d_{j,\nu}^{\nu} \\ &\quad + \sum_{\mu=M+1}^{M+N} \sum_{\nu=M+1}^{M+N} c_{i,\mu}^{*\mu} \langle \chi_{\mu} | \chi_{\nu} \rangle d_{j,\nu}^{\nu} \\ &= 0 \end{aligned}$$

The second and third terms are identically zero since $\langle \chi_{\mu} | \chi_{\nu} \rangle = 0$. For the first term, $c_{i,\mu}^{*\mu} = 0$ and for the fourth term, $d_{j,\nu}^{\nu} = 0$ (Table 2), removing each of those terms.

2.4.2 Overlap and Hamiltonian matrices

We derive in Appendix A.1 and A.2 expressions for the Overlap and Hamiltonian matrix elements between states of the two molecules A and B. The Overlap matrix can be written as:

$$\langle U | V \rangle = \langle U^A | V^A \rangle \langle U^B | V^B \rangle \quad (8)$$

From the expression, we see that the overlap matrix is *multiplicatively separable*.

In matrix form, this corresponds to:

$$\mathbf{S}_{AB} = \mathbf{S}_A \otimes \mathbf{S}_B \quad (9)$$

which reflects the use of a direct product basis.

The Hamiltonian matrix can be expressed as:

$$\begin{aligned} \langle U | \hat{H} | V \rangle &= \langle U^A | \hat{H} | V^A \rangle \langle U^B | V^B \rangle \\ &\quad + \langle U^B | \hat{H} | V^B \rangle \langle U^A | V^A \rangle \end{aligned} \quad (10)$$

In contrast to the Overlap matrix, the Hamiltonian matrix is *additively separable*.

In matrix form, this corresponds to

$$\mathbf{H}_{AB} = \mathbf{H}_A \otimes \mathbf{S}_B + \mathbf{S}_A \otimes \mathbf{H}_B \quad (11)$$

In the special case (orthogonal basis states) where $\mathbf{S}_A = \mathbf{1}_A$ and $\mathbf{S}_B = \mathbf{1}_B$, the equation reduces to the more familiar form[7]:

$$\mathbf{H}_{AB} = \mathbf{H}_A \otimes \mathbf{1}_B + \mathbf{1}_A \otimes \mathbf{H}_B \quad (12)$$

2.4.3 Size-Consistency

The generalised eigenvalue equations for the two molecules A and B individually are:

$$\mathbf{H}_A \mathbf{D}_A = \mathbf{S}_A \mathbf{D}_A E_A \quad (13)$$

$$\mathbf{H}_B \mathbf{D}_B = \mathbf{S}_B \mathbf{D}_B E_B, \quad (14)$$

and these define NOCI wavefunctions, and energies for the separated molecular systems. We now take $\mathbf{D}_{AB} = \mathbf{D}_A \otimes \mathbf{D}_B$ as a trial wavefunction of the combined systems using the direct product basis. In the combined system, the generalised eigenvalue equation is:

$$\mathbf{H}_{AB} \mathbf{D}_{AB} = \mathbf{S}_{AB} \mathbf{D}_{AB} E_{AB} \quad (15)$$

Expanding the LHS and comparing the expression, we get:

$$\begin{aligned} \mathbf{H}_{AB} \mathbf{D}_{AB} &= (\mathbf{H}_A \otimes \mathbf{S}_B + \mathbf{S}_A \otimes \mathbf{H}_B) (\mathbf{D}_A \otimes \mathbf{D}_B) \\ &= (\mathbf{H}_A \otimes \mathbf{S}_B) (\mathbf{D}_A \otimes \mathbf{D}_B) \\ &\quad + (\mathbf{S}_A \otimes \mathbf{H}_B) (\mathbf{D}_A \otimes \mathbf{D}_B) \\ &= (\mathbf{S}_A \mathbf{D}_A \otimes \mathbf{S}_B \mathbf{D}_B) (E_A + E_B) \\ &= \mathbf{S}_{AB} \mathbf{D}_{AB} (E_A + E_B) \end{aligned} \quad (16)$$

Hence, we can conclude that $E_{AB} = E_A + E_B$. We would like to reiterate that this proof rests upon the assumption that molecules A and B are far apart, and the additive separability of energy at large intermolecular distances implies *size-consistency*. Size-consistency is achievable here as the reference UHF state is size-consistent too. By localising spin orbitals on each molecule in a dimer, we have demonstrated formally that the NOCI approach can yield size-consistent results.

Molecule	u_i	v_i
A ($1 \leq i, j \leq P$)	$c_i^\mu = 0$ for $\mu \geq M + 1$	$d_i^\nu = 0$ for $\nu \geq M + 1$
B ($P + 1 \leq i, j \leq P + Q$)	$c_i^\mu = 0$ for $\mu \leq M$	$d_i^\nu = 0$ for $\nu \leq M$

Table 2: Summary of vanishing coefficients.

3 Results and Discussion

3.1 Computational Details

All calculations were performed using Q-Chem 5.3[47]. In-house Python codes were used to perform spin rotation on the sb-UHF states and to determine the irreducible representations spanned by the NOCI states found. Quantum Toolbox in Python (QuTiP) 4.3.1[48] was employed to simultaneously diagonalise representation matrices. 3D-rendering of molecules were produced with the IQMol software. The general approach for performing NOCI are as follows:

1. Run SCF metadynamics on a given molecule [Q-Chem]
2. Extract the lowest energy UHF solution (sb-UHF) and generate spin-rotated states from it [Python]
3. Read in the generated states and run NOCI [Q-Chem]
4. Perform symmetry analysis on the obtained NOCI states [Python]

3.2 Hydrogen molecule

We first investigate the properties of the method with the hydrogen molecule using the STO-3G basis set. The hydrogen molecule is stretched, with a bond length of 1.5\AA . We first use spin rotated states from the set of rotation operators, $\{\hat{R}(\frac{n\pi}{2}\hat{y})|n = 1, 2, 3, 4\}$ to generate NOCI states (Table 3). We have found that the number of states, and not the angle of rotation used, is of consequence to the efficacy of our method. Hence, the angle of rotation chosen will be standardised to be $\frac{2\pi}{m}$ where m is the number of spin-rotated states desired. Rotation about the y-axis privileges it and hence shall be taken as the reference axis. It follows that the $\langle S_y^2 \rangle$ and $\langle S_y \rangle$ values should be taken and the NOCI states expressed in terms of eigenkets $|S, M_{s,y}\rangle$, where S is the spin angular momentum and $M_{s,y}$ is the spin projection along the y-axis. From Table 3, we find that 3 NOCI states are obtained. The reduction in number of NOCI states as compared to the number of spin-rotated states reflects the linear dependence of fourth NOCI state on the three other NOCI states. However, we expect three states of $S^2 = 2$, corresponding to each of the $M_s = 1, 0, -1$ values.

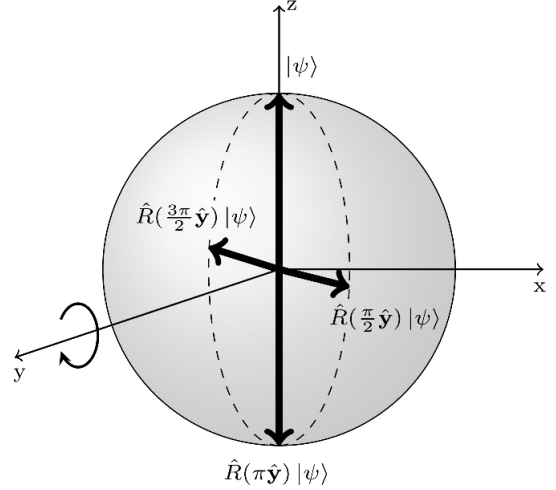


Figure 1: Pictorial representation of spin-rotation about the y-axis. The original state is taken to have spin along the z-axis. Rotation about the y-axis generates spin-rotated states which defines a plane, represented in the diagram by a disc.

The inability to find all of the three $S^2 = 2$ states using spin rotation about one axis can be reasoned as such: A rotation about an axis will generate states that spans a two-dimensional Euclidean space (Figure 1). As such, the spin state which exists perpendicular to the plane cannot be obtained. This is analogous to solving for a particle on a ring. For this well-known problem, the Hamiltonian is given by:

$$H = -\frac{\hbar^2}{2I} \frac{d^2}{d\phi^2} \quad (17)$$

and this has the general solution:

$$\Phi = Ae^{im\phi} + Be^{-im\phi} \quad (18)$$

Applying the periodic boundary conditions on the eigenfunction such that $\Phi(\phi) = \Phi(\phi + 2\pi)$, we get the result $m = 0, \pm 1, \pm 2, \dots$. This corroborates with our findings in Table 3, where only three states were found. State 1 corresponds to the $M_{s,y} = 0$ state while States 2 and 3 corresponds to linear combinations of the $M_{s,y} = 1$ and $M_{s,y} = -1$ states. A different perspective on the number of NOCI solutions possible is given in the Appendix. It is also possible to view this from a group-theoretic perspective[49]. From a well-known result in group

theory, Hilbert space can be partitioned into disjoint orbits[50]. Following seminal papers by Bacry[51–53], the orbits for $|0, 0\rangle$ and $|1, \pm 1\rangle$ spin states under the action of the rotation group are $SO(3)/SO(2)$, while the orbit for $|1, 0\rangle$ is $SO(3)/O(2)$. The orbits are different and hence they belong to disjoint sets of Hilbert space. Spin rotation about one axis is only sufficient in bringing out the spin states from one of the disjoint sets, hence only $|0, 0\rangle$ and $|1, \pm 1\rangle$ are observed upon spin rotation about the y -axis. A detailed mathematical analysis is beyond the scope of this paper, however.

With spin rotations about both the x - and y - axes using the set of spin rotations: $\{\hat{R}(\frac{n\pi}{2}\hat{\mathbf{y}})|n = 1, 2, 3, 4\} \cup \{\hat{R}(\frac{n\pi}{2}\hat{\mathbf{x}})|n = 1, 2, 3, 4\}$, we recover all of the expected states of the H_2 molecule (Table 4). For rotations about both the x - and y -axis (*vide infra*), the z -axis is privileged and $\langle S_z^2 \rangle$ and $\langle S_z \rangle$ values are taken instead. $M_{s,z}$ correspondingly refers to the spin projection about the z -axis. From the values of S^2 , $\langle S_y^2 \rangle$ and $\langle S_y \rangle$, we can deduce the nature of the NOCI states and give an eigenket representation (see Appendix A.3). This last state can be found .

The ground state singlet energy differs from the Full Configuration Interaction (FCI) value of $-0.9981494 E_h$ by 4.7 mE_h and can be attributed to the lack of dynamic correlation captured in our treatment.

States	S^2	$\langle S_y^2 \rangle$	$\langle S_y \rangle$	NOCI Energy
1	0.000	0.000	0.000	-0.9935034
2	2.000	1.000	0.000	-0.8905848
3	2.000	1.000	0.000	-0.8905848

Table 3: NOCI states of H_2 molecule. States found by spin rotation about y -axis. The y -axis is privileged by the axis of spin rotation and hence the the y -projection of the spin was taken. States 2 and 3 are linear combinations of the $M_{s,y} = 1$ and $M_{s,y} = -1$ states.

3.3 Collinear Hydrogen

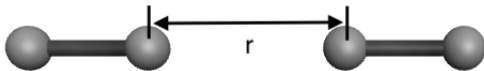


Figure 2: Collinear Hydrogen, $r = 10\text{\AA}$

We will consider the case where $r = 10\text{\AA}$ (Figure 2). Using the set of rotations $\{\hat{R}(\frac{n\pi}{2}\hat{\mathbf{y}})|n = 1, 2, 3, 4\}$, we find nine NOCI states. Denoting the coupled state from two separate molecules A and B with spin quantum numbers m and n respectively as $A^m B^n$, we expect there to be an upper limit of 16 states formed from $A^0 B^0$, $A^1 B^0$, $A^0 B^1$ and $A^1 B^1$ using

Clebsch-Gordan coupling (Table 5).

Given that we have found 3 states for a single molecule, we would expect 3^2 possible states in the corresponding dimer. These 9 states were indeed found (Table 6).

Spin states	Possible spins (S)
$A^0 B^0$	0
$A^0 B^1, A^1 B^0$	1
$A^0 B^2, A^2 B^0$	2
$A^1 B^1$	0, 1, 2
$A^1 B^2, A^2 B^1$	1, 2, 3
$A^2 B^2$	0, 1, 2, 3, 4

Table 5: Possible spins (S) for each spin state. This is found by using the Clebsch-Gordan series. For a spin state $A^m B^n$, S takes on the values $|m + n|, |m + n - 1|, \dots, |m - n|$

There are three unique energies found across the 9 states. State 1 is unique, States 2-5 are degenerate, and so are States 6-9. Comparing the values of NOCI energy in Table 6 and that in Table 3, we find that the NOCI energy is size-consistent, as we expect.

States	S^2	$\langle S_y^2 \rangle$	$\langle S_y \rangle$	NOCI Energy
1	0.000	0.000	0.000	-1.98689058
2	2.000	1.000	0.000	-1.88403040
3	2.000	1.000	0.000	-1.88403040
4	2.000	1.000	0.000	-1.88403040
5	2.000	1.000	0.000	-1.88403040
6	2.000	0.000	0.000	-1.78116950
7	6.000	4.000	0.000	-1.78116950
8	6.000	4.000	0.000	-1.78116950
9	2.000	0.000	0.000	-1.78116950

Table 6: NOCI states of collinear H_2 . States found by spin rotation about y -axis. A maximum of 9 (3^2) states can be found as there were only 3 states found in the hydrogen molecule.

3.4 Spin rotation about two axes

Although we were unable to obtain all of the possible spin states by rotation about one axis, the correct spin states can be found with two. Performing rotations with this set of rotations:

$\{\hat{R}(\frac{n\pi}{2}\hat{\mathbf{y}})|n = 1, 2, 3, 4\} \cup \{\hat{R}(\frac{n\pi}{2}\hat{\mathbf{x}})|n = 1, 2, 3, 4\}$, we find all 16 states (Table 7). The NOCI energies found have degeneracies in the ratio of 1:6:9, as we expect. We also see that the full possible 16 states have been found with the correct S^2 and S_z values. This demonstrates that the method is able to project out the various spin symmetry respecting components of the symmetry broken solution, and points to a possible way forward.

States	S^2	$\langle S_z^2 \rangle$	$\langle S_z \rangle$	NOCI Energy	Eigenket representation
1	0.000	0.000	0.000	-0.99344651	$ 0, 0\rangle$
2	2.000	1.000	1.000	-0.89058478	$ 1, 1\rangle$
3	2.000	0.000	0.000	-0.89058478	$ 1, 0\rangle$
4	2.000	1.000	-1.000	-0.89058478	$ 1, -1\rangle$

Table 4: NOCI states of H_2 molecule. States found by spin rotation about both x and y-axes. Having used both the x- and y- axes for spin rotation, the z-axis becomes the natural axis to take the spin projection.

States	S^2	$\langle S_z^2 \rangle$	$\langle S_z \rangle$	NOCI Energy	Eigenket representation
1	0.000	0.000	0.000	-1.98689058	$ 0, 0\rangle 0, 0\rangle$
2	2.000	1.000	1.000	-1.88403040	$\frac{1}{\sqrt{2}}(0, 0\rangle 1, 1\rangle + 1, 1\rangle 0, 0\rangle)$
3	2.000	1.000	-1.000	-1.88403040	$\frac{1}{\sqrt{2}}(0, 0\rangle 1, -1\rangle + 1, -1\rangle 0, 0\rangle)$
4	2.000	1.000	-1.000	-1.88403040	$\frac{1}{\sqrt{2}}(0, 0\rangle 1, -1\rangle - 1, -1\rangle 0, 0\rangle)$
5	2.000	1.000	1.000	-1.88403040	$\frac{1}{\sqrt{2}}(0, 0\rangle 1, 1\rangle - 1, 1\rangle 0, 0\rangle)$
6	2.000	0.000	0.000	-1.88403040	$\frac{1}{\sqrt{2}}(0, 0\rangle 1, 0\rangle + 1, 0\rangle 0, 0\rangle)$
7	2.000	0.000	0.000	-1.88403040	$\frac{1}{\sqrt{2}}(0, 0\rangle 1, 0\rangle - 1, 0\rangle 0, 0\rangle)$
8	2.000	1.000	-1.000	-1.78116950	$\frac{1}{\sqrt{2}}(1, 0\rangle 1, -1\rangle - 1, -1\rangle 1, 0\rangle)$
9	2.000	1.000	1.000	-1.78116950	$\frac{1}{\sqrt{2}}(1, 1\rangle 1, 0\rangle - 1, 0\rangle 1, 1\rangle)$
10	6.000	1.000	-1.000	-1.78116950	$\frac{1}{\sqrt{2}}(1, 0\rangle 1, -1\rangle + 1, -1\rangle 1, 0\rangle)$
11	6.000	1.000	1.000	-1.78116950	$\frac{1}{\sqrt{2}}(1, 1\rangle 1, 0\rangle + 1, 0\rangle 1, 1\rangle)$
12	6.000	4.000	2.000	-1.78116950	$ 1, 1\rangle 1, 1\rangle$
13	2.000	0.000	0.000	-1.78116950	$\frac{1}{\sqrt{2}}(1, 1\rangle 1, -1\rangle - 1, -1\rangle 1, 1\rangle)$
14	6.000	4.000	-2.000	-1.78116950	$ 1, -1\rangle 1, -1\rangle$
15	0.000	0.000	0.000	-1.78116950	$\frac{1}{\sqrt{3}}(1, 1\rangle 1, -1\rangle + 1, -1\rangle 1, 1\rangle - 1, 0\rangle 1, 0\rangle)$
16	6.000	0.000	0.000	-1.78116950	$\frac{1}{\sqrt{6}}(1, 1\rangle 1, -1\rangle + 1, -1\rangle 1, 1\rangle + 2 1, 0\rangle 1, 0\rangle)$

Table 7: NOCI states of collinear H_2 . States found by spin rotation about x and y-axes. All 16 possible spin states are found. The degeneracy of the solutions are 1,6 and 9, corresponding to the spin states A^0B^0 , $A(B)^0B(A)^1$ and A^1B^1 .

4 Stretched ethene

Using spin rotated states as a basis, we studied the dissociation of an ethene molecule into two carbenes. The dissociation process is modelled by elongating the C-C bond and leaving remaining bond lengths and bond angles constant. While we have attempted to localise the spin orbitals on the individual carbene fragment using Pipek-Mezey localisation, this approach breaks down as the C-C distance decreases. To circumvent this problem, ALMO were used to ensure that the spin orbitals are localised on each carbene fragment, allowing us to perform spin rotation on the individual fragments across all C-C distances. The ALMOs centred on each molecule are not orthogonal to each other

We first trace the two lowest energy sb-UHF solutions at a C-C distance of 1.5Å, and the results are plotted in Figure 3. Treating the ALMO solutions found at each geometry using SR-NOCI with the set of spin rotations: $\{\hat{R}(\frac{n\pi}{2}\hat{y})|n = 1, 2, \dots, 8\} \cup \{\hat{R}(\frac{n\pi}{2}\hat{x})|n = 1, 2, \dots, 8\}$, we have found a series of spin states, and the low-lying Singlet, Triplet and Quintet states have been plotted in Figure 4. The plot confirms the size consistency of the NOCI states, as the NOCI energies approaches the sum of the NOCI energies on the individual carbene fragments (see Supporting Information). It is worth noting that the size consistent property is extended to excited states as well.

Curiously, we observe that at small C-C distances, there are two singlet states, $S_0(1)$ and $S_0(2)$ found which are close in energy. The presence of multiple solutions found using ALMO is surprising, and we are unaware of any work on this problem. We were interested to know if the two singlet states found were are truly different or simply different approximations of the same state. To that end, we utilised spin-rotated states of both sb-UHF solutions as a basis for NOCI to consider the results of increasing the variational space. In general, this approach should not be size-consistent as we have increased the variational space used. From Figure 5 (Left), we observe that the increase in variational space does decrease the NOCI energy. However, this requires doubling the number of spin-rotated states used and the dissociation becomes size-inconsistent.

A more computationally efficient method would be to optimise NOCI states of the same spin. By taking the S_0 states from the two sb-UHF states and performing configuration interaction between these two states, we find that the resultant Singlet state is remarkably close to S_0 (Combined), the S_0

state found using both sb-UHF solutions (Figure 5 (Right)). At larger C-C bond distances, the two NOCI energies converge. We therefore obtain a close approximation to S_0 (Combined) using only two NOCI states, and the difference can be attributed to not having used all of the Singlet states found in the configuration interaction.

Figure 4 puts the equilibrium C-C bond length at around 1.45Å. We note that the experimental C-C bond length for ethene is 1.33Å. The discrepancy can be attributed to the lack of dynamic correlation and that the localised orbitals are not a good basis to capture the bonding between the carbene fragments.

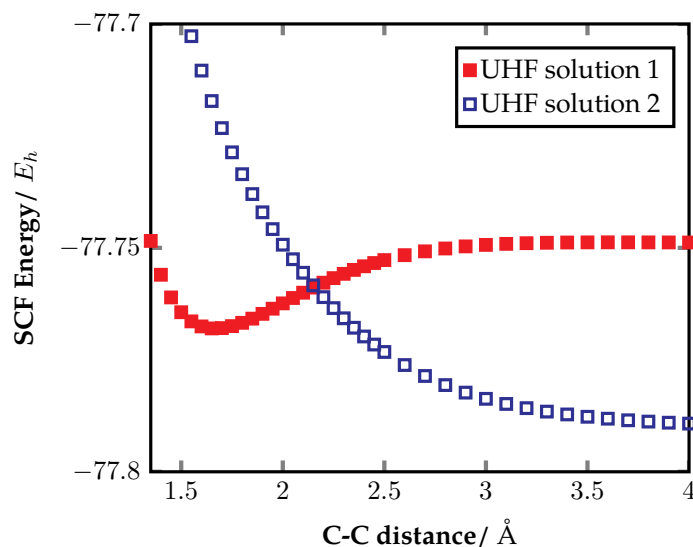


Figure 3: Plot of the two UHF solutions with ALMO across various C-C bond distances. These solutions are typically spin contaminated.

5 Comparison between MS-NOCI and SR-NOCI

In previous work done by the group, various SCF solutions were used as a basis for NOCI. We will compare the number of solutions used, energy and $\langle S^2 \rangle$ of the NOCI ground state found to demonstrate that the spin-rotated basis is a good alternative.

We shall use Fluorine, D_{4h} Cyclobutadiene, Alizarin Donor and Acceptor states which were previously used as model systems in research carried out by the group. A common set of rotations: $\{\hat{R}(\frac{n\pi}{4}\hat{y})|n = 1, 2, \dots, 8\} \cup \{\hat{R}(\frac{n\pi}{4}\hat{x})|n = 1, 2, \dots, 8\}$ would be used across the systems for consistency. The basis set used is consistent with those used in previous works. Table 8 summarises the difference in results between SR-NOCI against the previous method of MS-NOCI. Fluorine is well-known as a challenging system for computational chemistry due

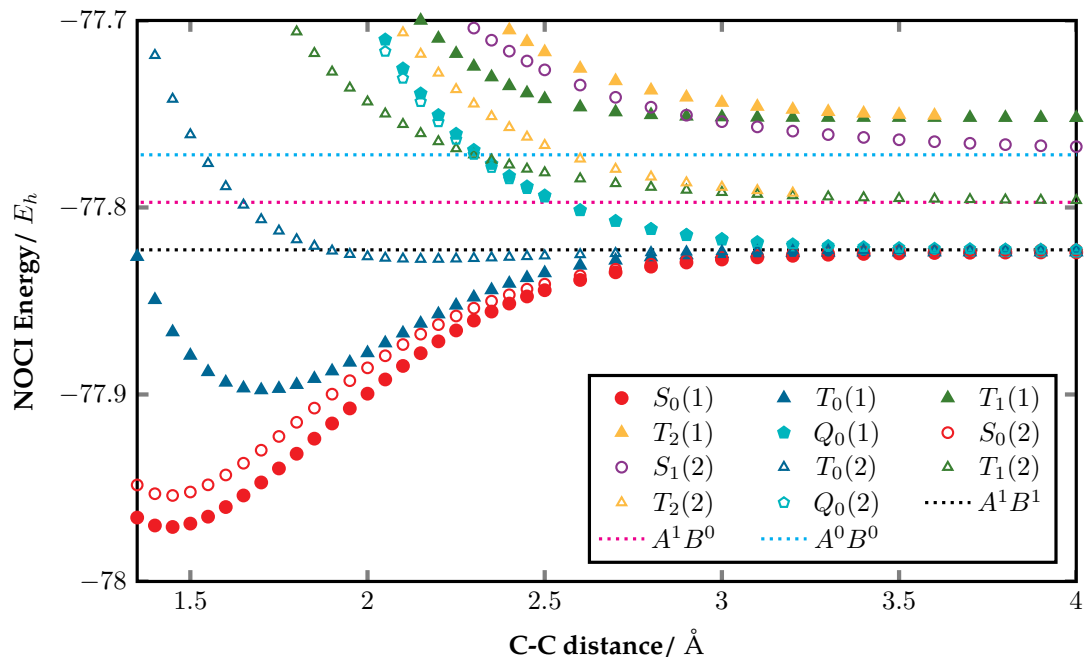


Figure 4: NOCI states found by performing SR-NOCI on the UHF solution 1 (Filled) and 2 (Empty) separately. Solution from which a spin state is derived is indicated in parentheses. The states are labelled in the format $X_p(q)$ where $X = S, T, Q$ for Singlet, Triplet or Quintet respectively. p numbers the states in order of energy (zero-based). q refers to the sb-UHF state from which the NOCI state is generated. $q = 1$ represents the UHF solution 1 in Figure 3. The dotted lines represents the asymptotic energies of the spin states. At larger C-C bond distances, the energy of the spin states tend towards the asymptotic energies, demonstrating that SR-NOCI is a size consistent method.

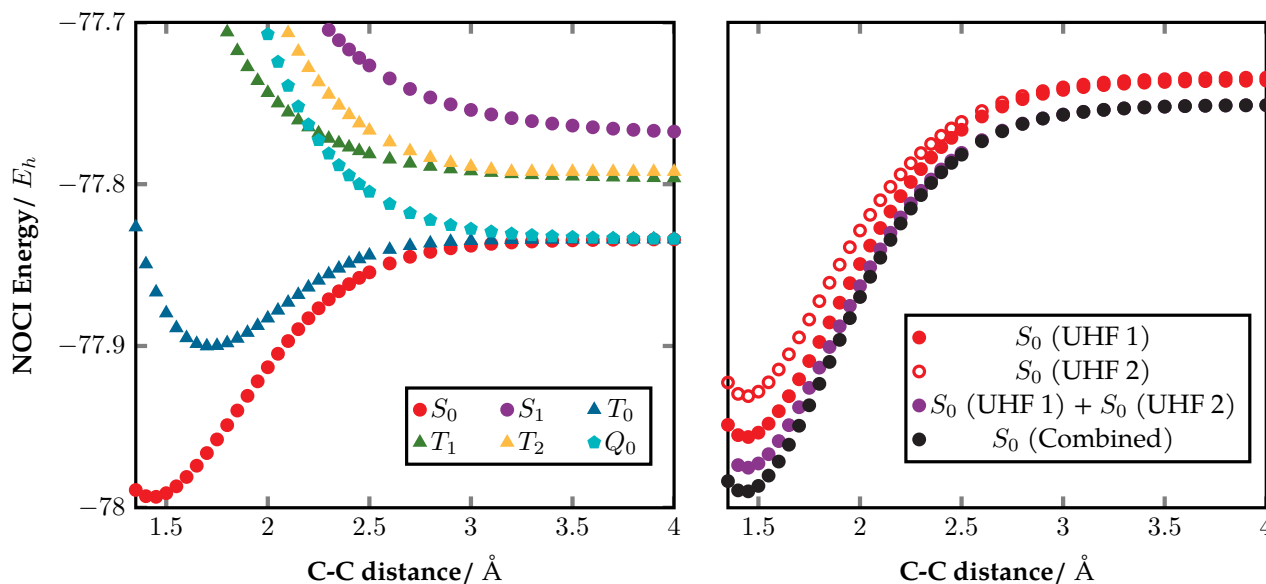


Figure 5: (Left) Dissociation curve of ethene using spin-rotated states of *both* UHF solution 1 and UHF solution 2. (Right) Magnified view of S_0 in the left plot, compared against the S_0 state found by coupling $S_0(1)$ and $S_0(2)$ in Figure 4. Difference in energy between S_0 (UHF 1) + S_0 (UHF 2) and S_0 (Combined) can be attributed to not having used all of the Singlet states found.

Molecule	MS-NOCI			SR-NOCI		
	Dimension of NOCI ^a	NOCI Energy	$\langle S^2 \rangle$	Dimension of NOCI ^b	NOCI Energy	$\langle S^2 \rangle$
$F_2^1(E_{min})^2$	3	-198.73848	0.002	14	-198.73770	0.000
$F_2^3(2\text{\AA})$	8	-198.77008	0.007	14	-198.76155	0.000
$F_2^3(8\text{\AA})$	8	-198.75051	0.007	14	-198.75497	0.000
D_{4h} Cyclobutadiene ³	12	-153.72075 ($^1B_{1g}$)	0.080	14	-153.72127 ($^1B_{1g}$)	0.000
	12	0.01630 ^c ($^3A_{2g}$)	2.006	14	0.01773 ^c ($^3A_{2g}$)	2.000
	12	0.06987 ^c ($^1A_{1g}$)	0.039	27 ^d	0.09463 ^c ($^1A_{1g}$)	0.0276
	12	0.12331 ^c ($^1B_{2g}$)	0.000	14	0.14570 ^c ($^1B_{2g}$)	0.000
Alizarin-Titanium (D) ⁴	30	-1984.69793 ^e	0.659	14	-1984.70549	0.004
Alizarin-Titanium (A) ⁴	30	-1984.69457 ^e	0.810	14	-1984.71074	0.067

Table 8: Comparison of data found using MS-NOCI against SR-NOCI

- ^a The dimensions is found from the number of HF solutions used. The previous method uses multiple HF solutions for NOCI. Whenever the solution used is a UHF one (UHF states with $M_s = 0$ are assumed), its spin-flipped partner is as well.
- ^b The dimensions is found from the number of spin rotations used. The dimension of 14 arises from the following set of rotations: $\{\hat{R}(\frac{n\pi}{4}\hat{y})|n = 1, 2, \dots, 8\} \cup \{\hat{R}(\frac{n\pi}{4}\hat{x})|n = 1, 2, \dots, 8\}$.
- ^c These energies corresponds to the excitation energy from their respective ground $^1B_{1g}$ states.
- ^d There is an increase of dimension by 13 as the solutions found by applying non-trivial operations of the D_{4h} group was used as well to restore spatial symmetry.
- ^e The energies here are slightly different from those previously reported. The discrepancy was due to the lack of phase correction after Löwdin Pairing in the previous Q-Chem code. This has since been rectified.
- ¹ 6-31G basis set was used.
- ² E_{min} is the lowest NOCI energy found across the F-F bond geometries sampled.
- ³ cc-pVDZ basis was used.
- ⁴ 6-31G* basis set was used.

to the high degree of both static and dynamic correlation. E_{min} of Fluorine found with the spin-rotated approach is in good agreement with MS-NOCI using 3 SCF states (Differing by $7.8 \times 10^{-4} E_h$). This suggests that the spin-rotated approach simply recovers static correlation.

For F_2 at 2\AA , we observe that SR-NOCI gives a higher energy ground state, suggesting that the use of one symmetry-broken UHF state is insufficient in capturing the dynamic correlation in Fluorine. As the bond length of F_2 increases to 8\AA , however, we see that the present method gives a slightly lower energy. This agrees with our understanding as the dynamic correlation between electrons on each F atom is made less significant at this bond length.

For D_{4h} Cyclobutadiene, the lowest two energy states (Singlet and Triplet) were found from applying spin rotation to the lowest energy sb-UHF state, the other two states found by applying spin rotation to the second and third lowest energy sb-UHF states, respectively. We find that the NOCI energies found from our approach is comparable to the ones previously reported, and does better than CIS or CASSCF approaches[27].

We were initially unable to obtain the A_{1g} state from the second-lowest energy sb-UHF state as there was significant spatial symmetry breaking which were

not found in the other two sb-UHF solutions. This can be overcome by the addition of 13 other solutions found by applying the non-trivial operations of the D_{4h} group to the sb-UHF solution[2]. However, as the addition of spatial symmetry-related solutions increases computational costs, we do not generally use them except in cases of significant spatial symmetry breaking.

The value of the spin-rotated approach can be more fully appreciated when we move on to larger systems. In larger systems, it is common to find many sb-UHF solutions and hence the selection of chemically relevant states is a non-trivial task. As with the example of both forms of the Alizarin-Titanium complex (Donor and Acceptor states, as defined in a previous work), the NOCI states found with MS-NOCI usually suffers from spin contamination. Using SR-NOCI, we have found Singlet ground states in each of the Alizarin-Titanium complexes which are lower in energy than previously reported. The improved spin purity of the NOCI states is heartening as it gives us more confidence that we are describing the correct spin states.

Previously, 30 SCF states were used, as compared to the current approach uses only 14 states to obtain a lower energy ground state which respects spin symmetry. This can therefore be useful in calculating

the spin states of large molecular systems which may be too computationally intensive with currently available methods.

6 Conclusion

We have conducted a study on the viability of using spin-rotated states as a basis for NOCI (SR-NOCI). Using this method, the energies found were comparable to those found with SCF metadynamics states as a basis (MS-NOCI). Our current approach comes with three additional advantages:

1. It is a black-box method where the same methodology can be used for molecular systems of various sizes, albeit with a change in number of spin rotations required.
2. Only one sb-UHF state is required to obtain NOCI states with static correlation recovered and possess good spin quantum numbers.
3. It offers the advantage of having a smaller dimension of NOCI in larger systems.

This method, however, only recovers the static correlation as it projects out the various spin components of a sb-UHF state. A further improvement can be made by employing perturbative methods such as NOCI-MP2[54, 55] or NOCI-PT2[56] to account for dynamic correlation.

We have also applied our method to the dissociation of an ethene molecule into two carbenes with the help of ALMO. The results show that the dissociation is size consistent and the states respect spin symmetry at each step of the dissociation. The overestimate of ethene’s equilibrium bond length is similarly attributed to the lack of dynamic correlation in our approach.

We can see a potential application of this work in Singlet Fission modelling[11–15, 57]. An important state in Singlet Fission is the correlated triplet state, $^1(TT)$, as denoted in literature[58]. This corresponds to a A^1B^1 system of $S = 0$ in our notation. We are also able to track the spin state as the molecular components A and B dissociate. This will enable us to follow the dissociation of the correlated triplet pair state into two independent triplets. The balanced description of both ground and excited state in our approach is beneficial to obtaining more accurate excitation energies, which is another important aspect of Singlet Fission research. We hope to apply this method to the modelling of these photochemical processes in a future work.

7 Acknowledgements

We would like to thank Dr. Hugh Burton and Bang Huynh for their helpful advice and discussions in the preparation of this manuscript. A.J.W.T. thanks the Royal Society for a University Research Fellowship (UF160398).

8 Author’s Note

Research data supporting this publication will be available on the University of Cambridge’s Apollo repository.

A Appendix

A.1 Overlap matrix

Following the exposition of Löwdin[59–61] and Mayer[36],

$$U = \hat{A}[u_1(1)\dots u_P(P)u_{P+1}(P+1)\dots u_{P+Q}(P+Q)] \quad (19)$$

$$V = \hat{A}[v_1(1)\dots v_P(P)v_{P+1}(P+1)\dots v_{P+Q}(P+Q)] \quad (20)$$

where \hat{A} is the anti-symmetrising operator. After some algebra, we get the following expression for the value of the overlap between states U and V :

$$\langle U|V \rangle = \sum_{R \in S_{P+Q}} (-1)^r \langle u_1|v_{R_1} \rangle \dots \langle u_P|v_{R_P} \rangle \langle u_{P+1}|v_{R_{P+1}} \rangle \dots \langle u_{P+Q}|v_{R_{P+Q}} \rangle \quad (21)$$

where S_{P+Q} is the full symmetric group of $P+Q$ elements, and r is the parity of the permutation.

This equation can be simplified as $\langle u_i|v_j \rangle = 0$ if u_i and v_j are spin orbitals on different molecules. Therefore, for the set of spin orbitals $\{u_i|i \in 1, 2, \dots, P\}$, only their inner product with $\{v_j|j \in 1, 2, \dots, P\}$ survives. Similarly, for the set of spin orbitals $\{u_i|i \in P+1, P+2, \dots, P+Q\}$, only their inner product with $\{v_j|j \in P+1, P+2, \dots, P+Q\}$ survives.

The equation therefore reduces to:

$$\begin{aligned} \langle U|V \rangle &= \left(\sum_{R_i \in S_P} (-1)^{r_i} \langle u_1|v_{R_1} \rangle \dots \langle u_P|v_{R_P} \rangle \right) \\ &\quad \left(\sum_{R_j \in S_Q} (-1)^{r_j} \langle u_{P+1}|v_{R_{P+1}} \rangle \dots \langle u_{P+Q}|v_{R_{P+Q}} \rangle \right) \\ &= \det(\mathbf{S}_{UV}^A) \det(\mathbf{S}_{UV}^B) \\ &= \langle U^A|V^A \rangle \langle U^B|V^B \end{aligned} \quad (22)$$

Since we can consider each of the sets above as permuting separately, the equation can be decomposed into a product form. Each of the terms corresponds to the overlap between states U and V centred on a

particular molecule (A or B).

A.2 Hamiltonian matrix

For the Hamiltonian matrix, we separate it into the one- and two- electron cases respectively.

For the one-electron case:

$$\begin{aligned}
\langle U|\hat{F}|V\rangle &= \sum_{ij}^{P+Q} \langle u_i|\hat{f}|v_j\rangle D(i|j) \\
&= \sum_{i,j=1}^P \langle u_i|\hat{f}|v_j\rangle \mathbf{S}^A(i|j) \det(\mathbf{S}_{UV}^B) \\
&\quad + \sum_{i,j=P+1}^{P+Q} \langle u_i|\hat{f}|v_j\rangle \mathbf{S}^B(i|j) \det(\mathbf{S}_{UV}^A) \\
&= \langle U^A|\hat{F}|V^A\rangle \langle U^B|V^B\rangle \\
&\quad + \langle U^B|\hat{F}|V^B\rangle \langle U^A|V^A\rangle
\end{aligned} \tag{23}$$

Where we used the fact that if u_i and v_j belongs to different molecules, $\langle u_i|\hat{f}|v_j\rangle = 0$. The decomposition of $D(i|j)$ can be understood with reference to Figure 6. For molecule A, $1 \leq i \leq P$ and $1 \leq j \leq P$. Therefore, the bottom right block of \mathbf{S}^B remains unchanged. The determinant of the whole matrix is the product of the determinant of the top left block and the bottom right block. The latter is $\det(\mathbf{S}_{UV}^B)$, while the former is simply the cofactor of block \mathbf{S}^A .

For the two-electron case:

$$\begin{aligned}
\langle U|\hat{G}|V\rangle &= \frac{1}{2} \sum_{ijkl}^{P+Q} \langle u_i u_j|\hat{g}|v_k v_l\rangle D(ij|kl) \\
&= \sum_{ijkl=1}^P \langle u_i u_j|\hat{g}|v_k v_l\rangle \mathbf{S}^A(ij|kl) \det(\mathbf{S}_{UV}^B) + \\
&\quad \sum_{ijkl=P+1}^{P+Q} \langle u_i u_j|\hat{g}|v_k v_l\rangle \mathbf{S}^B(ij|kl) \det(\mathbf{S}_{UV}^A) \\
&= \langle U^A|\hat{G}|V^A\rangle \langle U^B|V^B\rangle \\
&\quad + \langle U^B|\hat{G}|V^B\rangle \langle U^A|V^A\rangle
\end{aligned} \tag{24}$$

where $\langle u_i(1)u_j(2)|\hat{g}|v_k(1)v_l(2)\rangle$ is written as $\langle u_i u_j|\hat{g}|v_k v_l\rangle$ for the sake of brevity. Since $\hat{H} = \hat{F} + \hat{G}$,

$$\begin{aligned}
\langle U|\hat{H}|V\rangle &= \langle U|\hat{F} + \hat{G}|V\rangle \\
&= \langle U|\hat{F}|V\rangle + \langle U|\hat{G}|V\rangle \\
&= \langle U^A|\hat{F} + \hat{G}|V^A\rangle \langle U^B|V^B\rangle \\
&\quad + \langle U^B|\hat{F} + \hat{G}|V^B\rangle \langle U^A|V^A\rangle \\
&= \langle U^A|\hat{H}|V^A\rangle \langle U^B|V^B\rangle \\
&\quad + \langle U^B|\hat{H}|V^B\rangle \langle U^A|V^A\rangle
\end{aligned} \tag{25}$$

A.3 Forming the eigenket representation

The construction of spin eigenfunctions is well established in literature[62–64]. This section will provide a short summary on our approach to obtaining the eigenket representation of our SR-NOCI states.

A.3.1 Ladder Operators

The formation of the eigenket representation for triplet-pair states (states which can be expressed as a linear combination of $|1, a\rangle |1, b\rangle$ where $a, b = 1, 0, -1$) is well-known. From the $|1, 1\rangle |1, 1\rangle$ state, which is one of highest spin and spin multiplicity given the coupling of two triplets, we can apply the annihilation operator, \hat{J}_- which is defined by:

$$\hat{J}_- |J, M\rangle = \sqrt{J(J+1) - M(M-1)} |J, M-1\rangle \tag{26}$$

We can obtain all the nine triplet states in this manner. However, this method is not applicable for states that has a $|0, 0\rangle$ component as it has a different spin. A more general method will thus be described in the next subsection.

A.3.2 Projection onto the direct product basis

A more general way of getting at the eigenket representation of the dimer is to construct it from that of the corresponding molecule. Denoting a spin-rotated state of the molecule as $|\psi^{mol}(\theta)\rangle$ and the spin-rotated state of the dimer as $|\psi^{dimer}(\theta_A, \theta_B)\rangle$, where $\theta_{A(B)}$ represents the angle by which the spin of molecule A(B) is rotated. For the purposes of this section, the axis of rotation is assumed to be arbitrary, but kept consistent throughout.

From this relation,

$$|\psi^{dimer}(\theta_A, \theta_B)\rangle = |\psi^{mol}(\theta_A)\rangle \otimes |\psi^{mol}(\theta_B)\rangle \tag{27}$$

we can express the spin eigenket in terms of the spin-rotated states.

Noting that the SR-NOCI state (these are spin purified states) for the molecule can be written as:

$$|\Psi_i^{NOCI, mol}\rangle = \sum_k |\psi_k^{mol}\rangle p_{\cdot i}^k \tag{28}$$

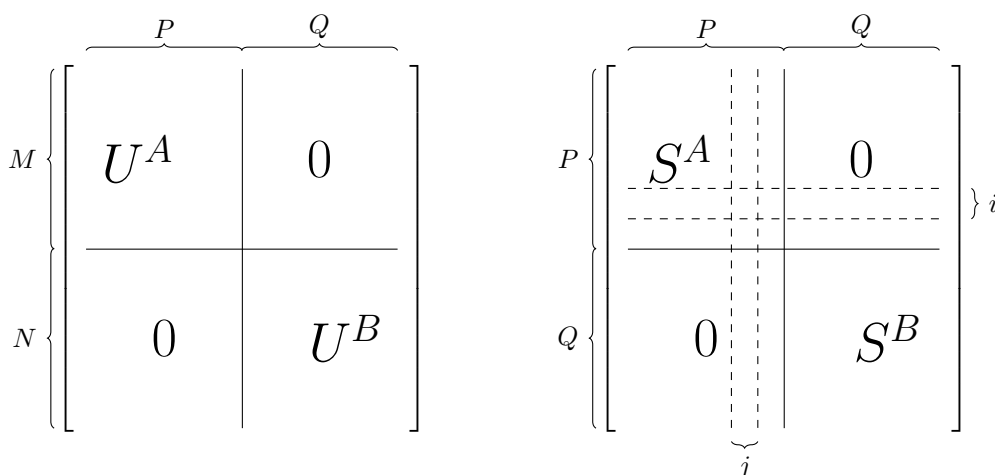


Figure 6: (Left) For a state U of a coupled system AB, the spin orbitals are localised on each molecule (A and B respectively) and arranged in a block diagonal fashion as shown. $U^{A(B)}$ corresponds to the spin orbitals of state U centred on molecule A(B). Each row represents an atomic orbital while each column represents a spin orbital. (Right) $S^{A(B)}$ is the overlap matrix centred on molecule A(B). The determinant of this block matrix gives the overlap between states U and V . The cofactor $D(i|j)$ is the determinant after a row i and column j has been removed. If the row and column are centred on molecule A(B), $S^{B(A)}$ remains unchanged. i and j must correspond to atomic orbitals on the same molecule or the associated terms will be vanishing.

Direct products of the spin states can be found by:

$$\begin{aligned}
 |\Psi_{i,j}^{basis}\rangle &= |\Psi_i^{NOCI,mol}\rangle \otimes |\Psi_j^{NOCI,mol}\rangle \\
 |\Psi_m^{basis}\rangle &= \left(\sum_k |\psi_k^{mol}\rangle p_{\cdot i}^k\right) \otimes \left(\sum_l |\psi_l^{mol}\rangle p_{\cdot j}^l\right) \\
 &= \sum_{kl} |\psi^{dimer}(\theta_A, \theta_B)\rangle (p_{\cdot i}^k \otimes p_{\cdot j}^l) \\
 &= \sum_k |\psi_k^{dimer}\rangle c_{\cdot m}^k
 \end{aligned} \quad (29)$$

where we have used a single index m for $|\Psi^{basis}\rangle$ instead for ease of notation in the second step, and indexed $|\psi^{dimer}(\theta_A, \theta_B)\rangle$ using k instead of the spin rotation angles. We can now express the SR-NOCI state, $|\Psi_j^{NOCI,dimer}\rangle$ as a linear combination of spin-rotated states:

$$|\Psi_j^{NOCI,dimer}\rangle = \sum_l |\psi_l^{dimer}\rangle d_{\cdot j}^l \quad (30)$$

To find the components of the direct product basis in the SR-NOCI state, we simply take the overlap between them:

$$\langle \Psi_m^{basis} | \Psi_j^{NOCI,dimer} \rangle = \sum_{k,l} c_m^* \cdot k \langle \psi_k^{dimer} | \psi_l^{dimer} \rangle d_{\cdot j}^l \quad (31)$$

This will project out the components of the SR-NOCI state which can inform us of the spin eigenket representation of each SR-NOCI state. It should be stressed that this approach only works when the two molecules in the dimeric system are well-separated insofar as the overlap between the two molecules approaches zero.

References

- (1) Szabo, A.; Ostlund, N. S., *Modern Quantum Chemistry: Introduction to Advanced Electronic Structure Theory*; Dover Publications Inc.: 1996.
- (2) Huynh, B. C.; Thom, A. J. W. *J. Chem. Theory Comput.* **2020**, *16*, 904–930.
- (3) Stuber, J. L.; Paldus, J. *Fundamental World of Quantum Chemistry: A Tribute to the Memory of Per-Olov Löwdin*, 2003.
- (4) Russ, N. J.; Crawford, T. D.; Tschumper, G. S. *J. Chem. Phys.* **2004**, *120*, 7298–7306.
- (5) Li, X.; Paldus, J. *J. Chem. Phys.* **2009**, *130*, 084110.
- (6) Amos, A. T.; Hall, G. G. *Proc. R. Soc. A* **1961**, *263*, 483–493.
- (7) Helgaker, T.; Olsen, J.; Jørgensen, P., *Molecular Electronic-Structure Theory*; Wiley-Blackwell: 2013.
- (8) Koga, N.; Yamashita, K.; Morokuma, K. *Chem. Phys. Lett.* **1991**, *184*, 359–362.
- (9) Andrews, J. S.; Jayatilaka, D.; Bone, R. G. A.; Handy, N. C.; Amos, R. D. *Chem. Phys. Lett.* **1991**, *183*, 423–431.
- (10) Lykos, P.; Pratt, G. W. *Rev. Mod. Phys.* **1963**, *35*, 496–501.
- (11) Smith, M. B.; Michl, J. *Chem. Rev.* **2010**, *110*, 6891–6936.
- (12) Smith, M. B.; Michl, J. *Annu. Rev. Phys. Chem.* **2013**, *64*, 361–386.
- (13) Casanova, D. *Chem. Rev.* **2018**, *118*, 7164–7207.
- (14) Havenith, R. W. A.; de Gier, H. D.; Broer, R. *Mol. Phys.* **2012**, *110*, 2445–2454.

- (15) Zimmerman, P. M.; Bell, F.; Casanova, D.; Head-Gordon, M. *J. Am. Chem. Soc.* **2011**, *133*, 19944–19952.
- (16) Scuseria, G. E.; Jiménez-Hoyos, C. A.; Henderson, T. M.; Samanta, K.; Ellis, J. K. *J. Chem. Phys.* **2011**, *135*, 124108.
- (17) Jiménez-Hoyos, C. A.; Henderson, T. M.; Tsuchimochi, T.; Scuseria, G. E. *J. Chem. Phys.* **2012**, *136*, 164109.
- (18) Smeyers, Y. G.; Doreste-Suarez, L. *Int. J. Quantum Chem.* **1973**, *7*, 687–698.
- (19) Cox, P. A.; Wood, M. H. *Theoret. Chim. Acta* **1973**, *41*, 269–278.
- (20) Cox, P. A.; Wood, M. H. *Theoret. Chim. Acta* **1976**, *41*, 279–285.
- (21) Mihálka, Z. É.; Surján, P. R.; Szabados, Á. *J. Chem. Theory Comput.* **2020**, *16*, 892–903.
- (22) Ye, H.-Z.; Voorhis, T. V. *J. Chem. Theor. Comput.* **2019**, *15*, 2954–2965.
- (23) Neuscammen, E. *J. Chem. Phys.* **2013**, *139*, 194105.
- (24) Thom, A. J. W.; Head-Gordon, M. *Phys. Rev. Lett.* **2009**, *101*, 193001.
- (25) Thom, A. J. W.; Head-Gordon, M. *J. Chem. Phys.* **2009**, *131*, 124113.
- (26) Jensen, K. T.; Benson, R. L.; Cardamone, S.; Thom, A. J. W. *J. Chem. Theory Comput.* **2018**, *14*, 4629–4639.
- (27) Burton, H. G. A.; Thom, A. J. W. *J. Chem. Theory Comput.* **2019**, *15*, 4851–4961.
- (28) Percus, J. K.; Rotenberg, A. *J. Math. Phys.* **1962**, *3*, 928–932.
- (29) Lefebvre, R.; Prat, R. *Chem. Phys. Lett.* **1967**, *1*, 388–390.
- (30) G.L. Bendazzoli; P. Palmieri; C. Zauli. *Chem. Phys. Lett.* **1971**, *8*, 556–558.
- (31) Sundstrom, E. J.; Head-Gordon, M. *J. Chem. Phys.* **2014**, *140*, 114103.
- (32) Nite, J.; Jiménez-Hoyos, C. A. *J. Chem. Theory Comput.* **2019**, *15*, 5343–5351.
- (33) Morrison, M. A.; Parker, G. A. *Chem. Phys. Lett.* **2007**, *40*, 445–450.
- (34) Viver, M. P. *Int. J. Quantum Chem.* **2019**, *119*, e25770.
- (35) Hait, D.; Haugen, E. A.; Yang, Z.; Oosterbaan, K. J.; Leone, S. R.; Head-Gordon, M. *J. Chem. Phys.* **2020**, *153*, 5435–5443.
- (36) Mayer, I., *Simple Theorems, Proofs and Derivations in Quantum Chemistry*; Springer: 2003.
- (37) Head-Gordon, M.; Maslen, P. E.; White, C. A. *J. Chem. Phys.* **1998**, *108*, 616–625.
- (38) Peierls, R. E.; Thouless, D. J. *Nuc. Phys.* **1962**, *38*, 154–176.
- (39) Laskowski, B.; Diamond, J.; Waleh, A.; Hudson, B. *J. Chem. Phys.* **1978**, *69*, 5222–5230.
- (40) Haider, Q.; Gogny, D. *J. Phys. G: Nucl. Part. Phys.* **1992**, *18*, 993–1022.
- (41) *The Nuclear Many-Body Problem*; Springer-Verlag Berlin Heidelberg: 1980.
- (42) Cohen-Tannoudji, C.; Diu, B.; Laloe, F., *Quantum Mechanics*; Wiley VCH: 2006; Vol. 2.
- (43) Boys, S. F. *Rev. Mod. Phys.* **1960**, *32*, 296–299.
- (44) Pipek, J.; Mezey, P. G. *J. Chem. Phys.* **1989**, *90*, 4916–4926.
- (45) Khaliullin, R. Z.; Head-Gordon, M.; Bell, A. T. *J. Chem. Phys.* **2006**, *124*, 204105.
- (46) Khaliullin, R. Z.; Cobar, E. A.; Lochan, R. C.; Bell, A. T.; Head-Gordon, M. *J. Chem. Phys. A* **2007**, *111*, 8753–8765.
- (47) Shao, Y. et al. *Molecular Physics* **2015**, *113*, 184–215.
- (48) Johansson, J.; Nation, P.; Nori, F. *Comp. Phys. Comm.* **2013**, *184*, 1234–1240.
- (49) Michel, L. *Rev. Mod. Phys.* **1980**, *52*, 617–651.
- (50) E Sá, N. B. *Journal of Physics A: Mathematical and General* **2001**, *34*, 4831–4850.
- (51) Bacry, H. *J. Math. Phys.* **1974**, *15*, 1686–1688.
- (52) Bacry, H. *J. Math. Phys.* **1978**, *19*, 1192–1195.
- (53) Bacry, H. *J. Math. Phys.* **1980**, *72*, 119–130.
- (54) Yost, S.; Head-Gordon, M. *J. Chem. Phys.* **2016**, *145*, 054105.
- (55) Yost, S.; Head-Gordon, M. *J. Chem. Theory Comput.* **2018**, *14*, 4671–4805.
- (56) Burton, H. G. A.; Thom, A. J. W. *J. Chem. Theory Comput.* **2020**, *16*, 5586–5600.
- (57) Wibowo, M.; Broer, R.; Havenith, R. W. A. *Comput. Theor. Chem* **2017**, *1116*, 190–194.
- (58) Miyata, K.; Conrad-Burton, F. S.; Geyer, F. L.; Zhu, X.-Y. *Chem. Rev.* **2019**, *119*, 4261–4292.
- (59) Löwdin, P.-O. *Phys. Rev.* **1955**, *97*, 1474–1489.
- (60) Löwdin, P.-O. *Phys. Rev.* **1955**, *97*, 1490–1508.
- (61) Löwdin, P.-O. *Phys. Rev.* **1955**, *97*, 1509–1520.
- (62) Pauncz, R., *Spin Eigenfunctions: Construction and Use*; New York ; London : Plenum Press: 1979.
- (63) Scholes, G. D. *J. Phys. Chem. A* **2015**, *119*, 12699–12705.
- (64) Tao, G.; Tan, Y. *J. Phys. Chem. A* **2020**, *124*, 5435–5443.